ORIGINAL ARTICLE



Laser direct fabrication and characterization of 3d lattice structures using continuous carbon fiber thermoset composites

Yuekun Chen¹ · Honghua Qian² · John Pappas¹ · Guoliang Huang² · Xiangyang Dong¹

Received: 2 May 2024 / Accepted: 21 June 2024 © The Author(s), under exclusive licence to Springer-Verlag London Ltd., part of Springer Nature 2024

Abstract

Continuous carbon fiber reinforced thermoset composites are high-strength, lightweight materials with high temperature and corrosion resistance that can be widely used in aerospace and other fields. Direct manufacturing of complex lattice structures remains challenging for manual assembly or existing additive manufacturing (AM) technologies. In this study, we developed a novel strategy to directly cure and print continuous carbon fiber (CCF) thermoset composite lattice structures under high laser intensity. Taking advantage of dual-cure characteristics of the photopolymer resin being used in this study through ultraviolet (UV) and thermal curing, 3D printed complex CCF lattice truss structures are self-supporting with rapid laser curing of the resin matrix material, thus eliminating the necessity of using support structures during 3D printing. The mechanical properties of the 3D printed carbon fiber lattice structure were experimentally measured through compression tests. The maximum compressive strength and the maximum compressive modulus were found to be 2.28 MPa and 4.48 MPa, respectively. A good agreement was also found in comparison with numerical simulations. With the AM method described here, to the best of our knowledge, this is the first study presenting direct 3D printing and characterization of CCF lattice structures with thermoset composites. It is also the first investigation to successfully print thermoset composite lattice structures and analyze their mechanical properties. It was also found that high laser intensity has a significant impact on the curing of thermoplastic materials. This method of laser printing and the choice of materials could serve as a basis for future research on thermoset composites. The findings open new avenues and provide insights in design and manufacturing of complex lattice structures using continuous carbon fiber reinforced thermoset composites.

Keywords Continuous carbon fiber · Additive manufacturing · Lattice structure · Thermoset composites

1 Introduction

Continuous carbon fiber reinforced polymer (C-CFRP) composites are composed of continuous fibers as a reinforcing material and various polymer as a matrix [1, 2]. The main properties of C-CFRPs, such as high strength-to-weight ratio, stiffness, and load-bearing capacity, combined with excellent fatigue resistance, corrosion resistance and wear resistance, are all derived from the reinforcing fibers [1, 3]. However, it remains challenging to manufacture complex

Miangyang Dong Xiangyang.Dong@asu.edu

Published online: 04 July 2024

C-CFRP composite parts such as lattice structures. Lattice structures are the most typical complex structure, which are formed by a spatially periodic array of unit cells with edges and faces [4, 5]. As lightweight structural designs, lattice structures save energy, material, optimizes the support structure volume, build time, and adjusts the build direction [6, 7], thereby effectively reducing energy consumption and material loss for the fabrication process [8]. Currently, lattice structures have many applications in real-life. The suspension arm in the front wheel assembly of a vehicle has improved strength and reduced weight after lattice structure optimization [9]. Fan blades with lattice structures are 27-64% lighter than solid structures, and the "strength/ mass" ratio is improved compared to solid metal [10]. A prototype wing segment of Unmanned Aerial Vehicles (UAVs) with a 3D printed lattice structure enables optimized design and development of motion flexibility [11]. However, difficulty in joining and assembling composite parts has severely



School of Manufacturing Systems and Networks, Ira A. Fulton Schools of Engineering, Arizona State University, Mesa, AZ 85212, USA

Department of Mechanical and Aerospace Engineering, University of Missouri, Columbia, MO 65211, USA

limited the implementation of lattice structures for industrial applications [12]. Preparation of C-CFRP lattice structures with high strength and complexity have been investigated in recent studies.

Among others, manual assembly and additive manufacturing (AM) methods have been used for fabrication of 3D lattice structures. The main methods for manually assembling lattice structures include hot press molding [13], stitching [14], snap-fitting [15–17], and weaving [18–20]. Guan et al. [21] explored a method of inserting carbon fiber (CF) prepreg into a concave silicone rubber mold with heating and curing to create inner and outer trusses. Lattice structures were then formed by inserting the cured inner trusses into the outer trusses. McClintock et al. [19] proposed the usage of crocheting and sewing techniques. CF tows were pre-impregnated with resin and woven onto a jig. After high-temperature curing, the connection with the jig was cut off to obtain the lattice structure. However, manual assembly has complicated steps and long preparation cycles, limiting its application in mass production. Differences in geometry, defects, and massscaling also caused large variations between experimental and finite element (FE) simulation results [19].

Compared with manual assembly of functional lattice structures, AM has recently been extensively used to prepare C-CFRP lattice structures due to its unique capabilities of fabricating complex structures [22]. AM provides better geometric control and predictability, while providing the ability to achieve a complex spatial distribution of material properties for lattice structures [23, 24], making the capability of 3D printed lattice structures significantly enhanced over other structures with equivalent porosity [23, 25]. Several recent studies have designed auxiliary technologies to assist additive methods in fabricating C-CFRP lattice structures. Different matrix materials have also been used to achieve preparation of complex structures. Wang et al. [26] proposed a dual-material 3D printing method to fabricate free-hanging lattice structures with thermoplastics. CF and polylactic acid (PLA) were co-extruded from the nozzle, and after being cooled by the fan, a triangle lattice truss core was printed. However, their study only prepared a parallel triangle truss core and did not consider more complex lattice truss structures. Liu et al. [27] and Zhang et al. [28] expounded a cooling air flow-assisted method to 3D print free-hanging continuous fiber-reinforced thermoplastics. However, a low specific modulus for the printed lattice structure was reported and was attributed the low modulus of the PLA matrix [27]. Li et al. [29, 30] developed technology for 3D printing with CF reinforced filament using microwave heating, which was used to print C-CFRP lattice structures. Microwaves were converted into transverse electric and magnetic field (TEM) waves through the coaxial resonant applicator. The magnetic field of the TEM wave induced current in the CF, generating Joule heating, and caused rapid heating of the impregnated CF reinforced polyamide filament, while other components remained at room temperature [29]. However, high-speed printing also caused CF deformation. At the same time, imprecise control of microwave power caused temperature fluctuations which increased difficulty of the AM process. Zhang et al. [31] reported a 3D printing process in which the CF path was continuously printed from the origin to the vertex of the tetrahedron. Thermoplastic resin and water-soluble resin were used as extrusion materials while support blocks were implemented to maintain the shape of the lattice structures during printing. However, using support blocks to maintain the position of struts and dangling stages also increased the complexity of the manufacturing processes and may limit its applications in fabricating complex lattice structures.

Thermoplastic composites generally do not have the stiffness and strength required for high-performance applications [32]. Compared to thermoplastic composites, thermoset polymers can form irreversible and stable chemical bonds after curing [33]. Thermoset polymers possess cross-linked polymer networks that provide good thermal and chemical stability as well as high mechanical properties [1, 33, 34]. The teams of He et al. [32], Abdullah et al. [35] and Jiang et al. [36] studied direct ink writing (DIW) technology to prepare continuous fiber reinforced thermoset composites. Extruded printable inks with fiber reinforcement were cured under ultraviolet (UV) light to form curved paths and complex structures, such as lattice structures and 3D curved surfaces. The overall mechanical properties of the composite material were greatly improved after a post-heat treatment [32, 36], which, however, also increased the fabrication cycle time. The group of Yourdkhani presented laser-curing of continuous carbon fiber impregnated with a thermoset resin and printed a composite beam in mid-air [37]. The realization of single-layer, multilayer or parallel free-hanging structures by high laser intensity was investigated. However, the fabrication of lattice structures with laser-cured thermoset composites has not been studied, to the best of our knowledge. Preparation of lattice structures relies on precise design and control of print toolpath and intersection locations during printing while continuous fibers in the cured thermoset composite reinforce the polymer structure.

In this study, we propose a new laser 3D printing method to directly fabricate continuous CF reinforced thermoset composite lattice structures without additional setup such as supporting structure, tooling, or post-processing steps. With the dual-cure characteristics of the photopolymer resin selected here, we are able to fully cure the thermoset composite extrudate directly under high UV laser intensity during 3D printing and thus fabricate 3D lattice structures reinforced with continuous carbon fibers. Through studying design and control of print toolpath, the impregnated thermoset composite is cured into a triangle structure and is further stacked into a 3D pyramid lattice structure. The



mechanical properties of the 3D printed lattice structure are characterized through compression tests and also compared between experimental measurements and numerical simulations. To the best of our knowledge, this is the first study presenting additively manufactured 3D lattice structure using thermoset composites and reporting corresponding mechanical characterization results.

2 Materials and methods

2.1 Material preparation

Polyacrylonitrile (PAN)-based CF (Thornel T300, 3 K) was used in this study due to its high strength and high modulus. The photopolymer resin (LOCTITE 3D 3955, 385–405 nm wavelength) was used as the matrix material. Before 3D printing, the resin was first heated in an oven at 80 °C for a minimum of 4 h to lower its viscosity and improve the impregnation of the CF bundle in fabrication of thermoset composites. Thus, the resin was maintained at 80 °C to facilitate resin infusion and composite printing throughout the experimentation.

2.2 Experiment setup

The schematics of the experimental setup used in this study is shown in Fig. 1. The as-received carbon fiber bundle was

first pre-impregnated by passing through a photopolymer resin bath at a constant temperature of 80 °C within a heated amber syringe. The pre-impregnation process promoted the bonding between individual CF and the thermoset resin [38] before being deposited on the glass substrate. A diameter of 1 mm for the prepreg fiber tow was obtained in this study after passing through the nozzle (Ramé-hart Instruments Co. gauge 18 nozzle, 0.84 mm inside diameter) with an average fiber volume fraction of 26 vol.%. It should be noted that the fiber volume fraction could be controlled by varying the nozzle size. To reduce the drag force on the fiber bundle and to facilitate fiber impregnation [39, 40], a tilt angle (ω) of 45 ° was used in this study following our preliminary studies of using the selected photopolymer resin. The thermoset composite extrudate was then deposited and cured by a 1.6 W UV laser (450 nm wavelength). A rectangular laser beam profile was implemented in this study with a laser spot size of 4.3 mm and 1.1 mm. The longitudinal direction of the laser beam (c), i.e., 4.3 mm, was aligned with the print direction to further improve the thermoset composite curing processes. The offset distance (φ) between the nozzle and the laser spot (center) was maintained at 5.4 mm to avoid premature curing of the thermoset rein and thus clogging the nozzle during deposition. A relatively low printing traverse speed of 10 mm/min was used to promote complete curing of the thermoset composite and minimize potential damage on the overlapping toolpaths. It is worth noting that the print speed can be further improved if a higher laser power is used.

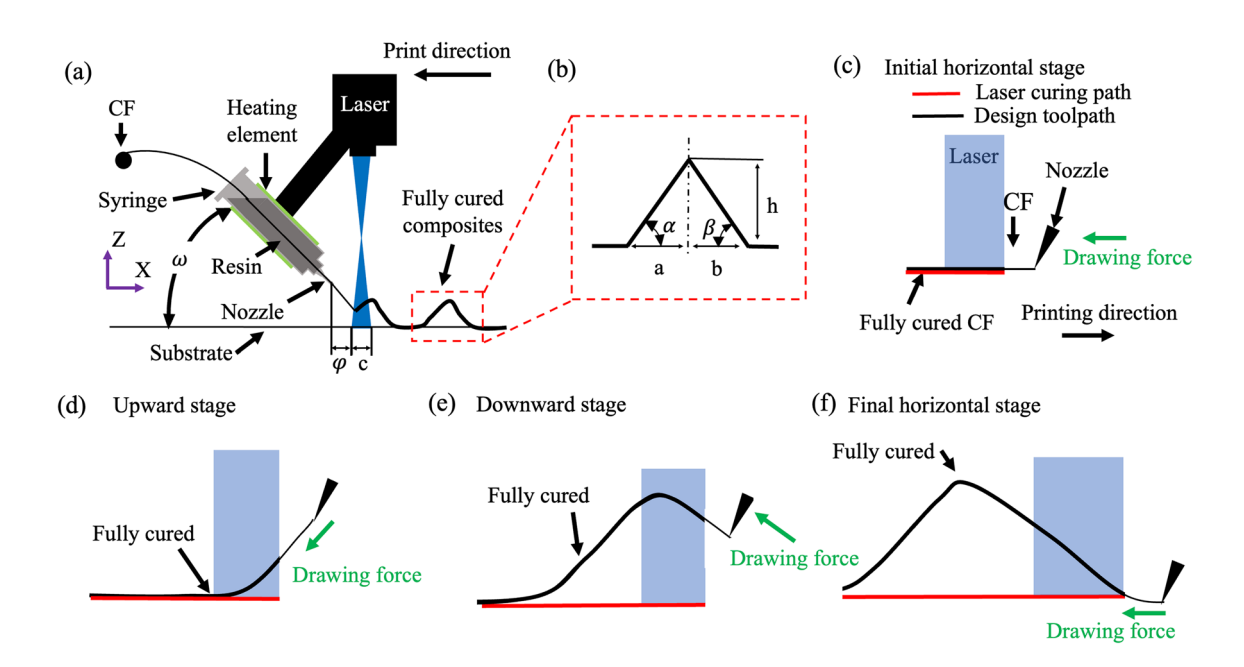


Fig. 1 Schematics of the experimental setup and printing processes. a shows an overview of the laser direct 3D printing setup. A toolpath of a single triangle lattice truss core is highlighted in (b). (c)-(f) show

the initial horizontal stage, the upward stage, the downward stage, and the final horizontal stage, respectively, during printing of the triangle truss structure



2.3 Mechanical testing, modeling setup, and characterization

To measure the mechanical properties, a three-dimensional 2×2 lattice structures was prepared with a side length of 50 mm. The distance between the vertices of two adjacent lattice cells was 21 mm. The 3D printed lattice structure was then placed in a sandwich construction to measure compressive forces normal to the composite sandwich surface. The glass substrate used during printing was directly used as the bottom plate of the sandwich structure. A same glass plate was attached to the top of the lattice structure with an adhesive (Gorilla super glue, impact-tough formula), forming a sandwich construction with top and bottom glass plates used for compression testing. The compression test of the constructed 2 × 2 sandwich core was subjected to an external compression force in the ADMET eXpert 2600 testing machine at a head displacement rate of 0.25 mm/min, based on the ASTM C365/C365M-05 standard. A total of 3 specimens were tested. Failure criteria was not reached until the sandwich core material was damaged due to either fracturing or Euler buckling.

To compare with experimental measurements, numerical simulations were also performed by numerical modeling of the lattice sandwich structures in COMSOL Multiphysics. The lattice geometry was aligned with the design parameters, using the 2×2 lattice structure. A flat plate was modeled beneath the lattice with the fixed boundary condition, and external force was applied to the top surfaces of the lattice to simulate the actual loading process in the experiment. In the simulation, the bottom plate was fixed with a high modulus (small deformation). In the experimental tests, the top plate was glued on the top of the lattice structure to distribute the loading force uniformly. Our preliminary numerical simulations showed that the deformation or strain experienced by the top plate was much smaller than that of the lattice structure itself, so the top plate was neglected during the simulation to improve the computational efficiency. The Young's modulus used in the simulation was determined by curve fitting the experimentally measured compression data of the lattice. The finite element model was meshed with 979,102 tetrahedral elements, with a maximum size under 0.1 mm. The geometrical nonlinearity is considered in the finite element model.

To characterize the cured thermoset composite samples, differential scanning calorimetry (DSC) analysis was performed on a high-performance differential scanning calorimeter (TA Instruments, DSC 250) in accordance with the ASTM E2160 standard. DSC experiments were performed with a ramp rate of 10 °C per minute with ultra-high purity nitrogen flowing continuously at 40 mL per minute. Prior to DSC testing, samples were hermetically sealed in aluminum containers (TA Instruments, Tzero pans and lids) with the

mass of each sample maintained between 4.9 mg to 5.1 mg. Analysis of results was performed with thermal analysis software (TA Instruments, TRIOS software).

3 Results and discussion

3.1 Toolpath design and fabrication of a single triangle lattice structure

As shown in Fig. 1b, the highlighted toolpath of the single triangle truss core consisted of the left half base (a), the right half base (b), the height of the core (h), the left half base inclination angle (α) , and the right half base inclination angle (β) . There were two paths in this method described by the laser cured path and design toolpath. The study analyzed the design toolpath to better understand the shape of the laser cured path. Due to the selected offset distance (φ) between the laser beam and the nozzle, there was deviation between the shape of the design toolpath and the laser cured path. Therefore, the four stages of the design toolpath were analyzed in detail to better understand the formation of the lattice structure and to achieve the desired lattice geometries.

The 3D printed toolpath can be divided into four stages including the initial horizontal stage, upward stage, downward stage, and final horizontal stage [26], as shown in Figs. 1c-f, respectively.

- Initial horizontal stage: the thermoset composite materials was extruded from the nozzle along the print direction and deposited onto the glass plate by laser curing. During this entire stage, the paths of the laser and the nozzle were both entirely along the X direction.
- Upward stage: The nozzle executed the upward stage according to the design toolpath while the laser spot lagged behind and was still on the horizontal stage due to the offset distance φ . The nozzle had two displacement components, along the Z direction and the X direction, forming an angle α with respect to the glass plate. The direction of movement of the laser was along the X-axis until the laser spot reached the inclined extrudate, where it had components along the X direction and Z direction. The laser spot size projected onto the inclined extrudate in the upward stage was $\frac{c}{\cos \alpha}$.
- Downward stage: The nozzle began to enter the downward stage. However, the laser curing path was still in the upward stage of the extruded composite. The nozzle moved in the positive X direction and the negative Z direction. Movement of the laser along the negative Z direction had no obvious effect on curing the composite materials, which was only affected by displacement along the positive X direction. The distance φ between the nozzle and the laser caused the composite materials between



- the nozzle and the laser to not be cured immediately, and the CF would be pulled in the negative Z direction by drawing force. Therefore, the height of the lattice structure was expected to be lower than the design path.
- Final horizontal stage: The nozzle entered the horizontal stage, while the laser remained in the downward stage. The projected laser spot size onto the extruded composite materials of the downward inclined path was $\frac{c}{\sin \beta}$. The design toolpath moved along a distance of φ along the X direction before the laser curing path entered the horizontal stage.

As discussed above, due to the offset distance φ between the nozzle and the laser, there was a delay in the laser curing path, which was expected to lead to the deviation from the design toolpath. Therefore, the shapes of two single-triangle tool paths, forming symmetric triangles and asymmetric triangles, were also compared using the same dimensions for the height (h) and the base length, i.e., the left half base (a) and the right half base (b), to understand how to modify print toolpath to achieve the desired lattice geometry. The schematic diagrams of the design paths are shown in Fig. 2. The design paths of the symmetric and asymmetric triangle paths were represented by dotted lines. The offset distance (φ) between the laser and the nozzle along the x direction remained as the same while the nozzle moved

along the design toolpath until it reached the vertex of the symmetric triangle (Fig. 2a). When the nozzle entered the downward stage of the symmetric triangle path, the laser did not cure the vertex, and the cured path for the symmetric structure deviated from the actual path due to the drawing force (Fig. 2b and c). In the downward stage, the two nozzles were at the same position in the X direction, but the position of the nozzle with the asymmetric path was higher in the Z direction than that of the symmetric path. Therefore, the actual height of the asymmetric path would be higher than the symmetric triangle path (Fig. 2d). The nozzle entered the final horizontal stage, and the laser curing path was delayed by the offset distance φ before entering the horizontal stage. The drawing force caused the CF to continue moving a certain distance along the X direction until the laser fully cured and deposited the thermoset composite materials onto the substrate. Ultimately, the actual length of the base of the triangle would be longer than the design tool path (Fig. 2e).

To validate the analysis above, the target dimensions of a triangle lattice structure were selected with a height (h) of 5 mm, and a total length of the base (a+b) of 15 mm as shown in Fig. 3a). Several sets of parameters were designed for further research to better understand the difference between the paths of symmetric and asymmetric triangles. The distance between the vertices of two adjacent lattice cells was 21 mm. The parameters of the modified path and

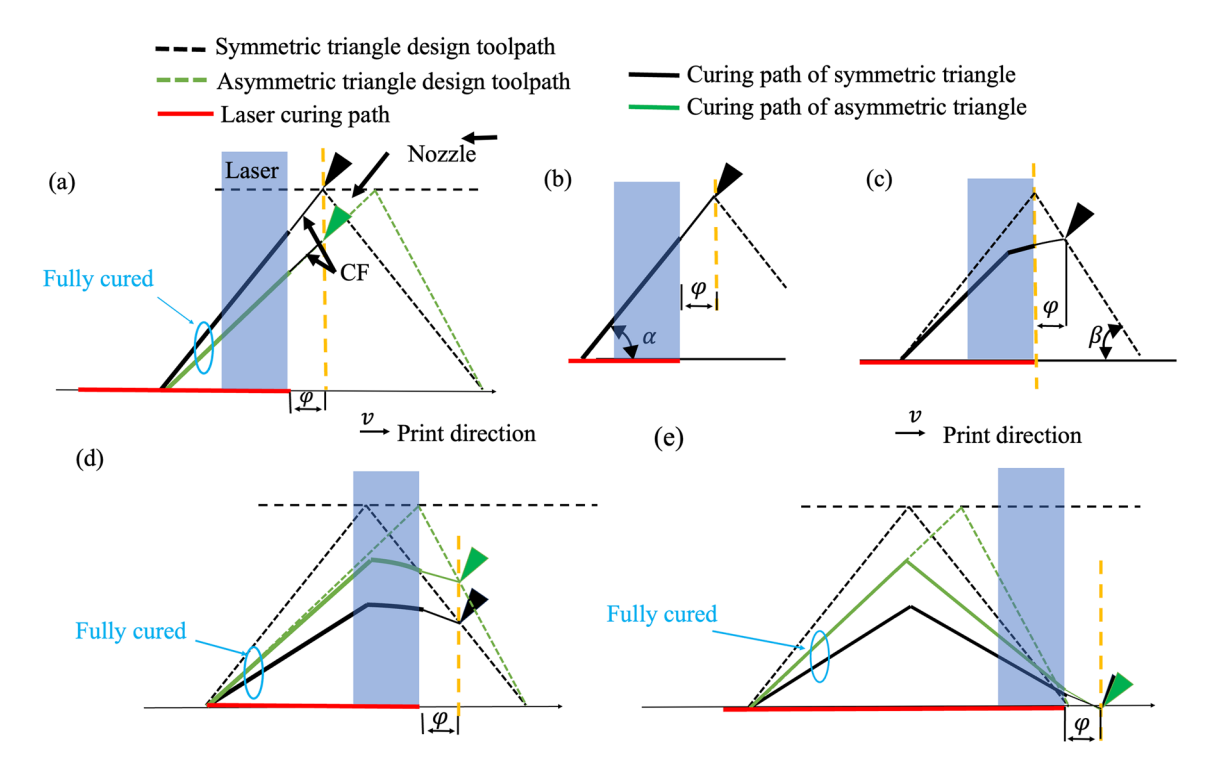


Fig. 2 The difference between symmetric and asymmetric triangle paths, (a)-(b) The nozzle was moved to the vertex of the symmetric triangle, (c)-(d) the nozzle was at the downward stage, (e) the nozzle was at the final horizontal stage



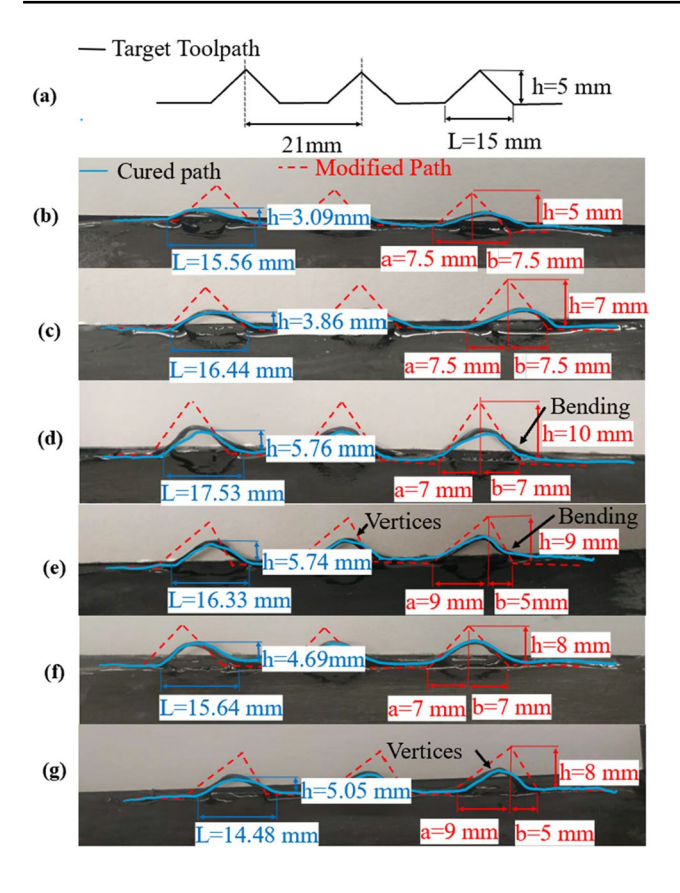


Fig. 3 3D printing a single triangle toolpath: **a** Target path. **b** The cured path under the target toolpath. Modified toolpath (**c**) symmetric triangle lattice truss core: h=7 mm, (**d**) symmetric triangle lattice truss core: h=10 mm, (**e**) asymmetric triangle lattice truss core: h=8 mm. **g** Asymmetric triangle lattice truss core: h=8 mm.

corresponding errors are summarized in Table 1. Figure 3b-g show the different modified paths and their cured paths. Figure 3b shows the printed path using the target path for nozzle movement. The height of the cured path was 1.91 mm lower than the target path, where the cured path formed a small curve. The target path was achieved by adjusting the dimensions of the triangle height and base and thereby changing the shape of the designed triangle.

The design paths in Fig. 3e and g were asymmetric triangles; however, the upward stage and the downward stage of the cured path were relatively symmetric. The cured path formed a vertex, and the shape was closer to a triangle. As the height of the triangular lattice increases, CF deforms and bends in the downward stage under drawing force. The designed height in Fig. 3d was 10 mm while the cured height was 5.76 mm, thus the height was 42% lower than the modified path, which was closer to the target path. was a slight bend in the downward stage. The size of the base increased to 17.53 mm. The base and height of the cured path in Fig. 3c, f, and g were closer to the target requirements. The height of the actual path was approximately 5 mm and formed the uniform curve. A more precise control of the target toolpath preparation could be achieved through a robotic arm to reduce the percentage error of the target path with multi-directional print methods.

When the triangle height was 8 mm, the measured heights of the two methods were 4.69 mm and 5.05 mm, respectively, as shown in Fig. 3f and g. The cured path at the top of the symmetric triangle was much smoother, with a gentle curve at the vertex. The asymmetric modified path enabled the preparation of high-height toolpaths, suitable for paths with a height of $h \ge 9$ mm or for realizing a toolpath with a sharp curve at the vertex. The parameters of the symmetric modified paths resulted in an actual cured path closer to the target path. The gentle curve at the top was conducive to overlap for printed multi-layer paths and was suitable for printing samples with h < 8 mm. However, there was an offset in the actual cured path of the CF bundle. The drawing force of the extrusion nozzle caused the actual path of the cured CF bundle to shift, especially in toolpaths with a large curvature [38]. Deformation occurred in the downward stage and this phenomenon was inevitable since friction at the edge of the nozzle resulted in greater drawing force for the deposited composite material. The CF bundle was under tension due to the drawing force of the deposited composite material [41]. Compared with the upward stage, the tension in the downward stage was much higher than that of the upward stage. Therefore, the CF in the downward stage

Table 1 Parameters of paths of the symmetrical triangle and the asymmetrical triangle

| Toolpath # | Design parameters (mm) | | | Printed parameters (mm) | | Percent error (%) from the target dimensions | |
|------------|------------------------|-----|----|-------------------------|------|--|------|
| | a | b | h | L | h | L | h |
| b | 7.5 | 7.5 | 5 | 15.56 | 3.09 | 3.7 | 38.2 |
| c | 7.5 | 7.5 | 7 | 16.44 | 3.86 | 9.6 | 22.8 |
| d | 7 | 7 | 10 | 17.53 | 5.76 | 16.9 | 15.2 |
| e | 9 | 5 | 9 | 16.33 | 5.74 | 8.9 | 14.8 |
| f | 7 | 7 | 8 | 15.64 | 4.69 | 4.3 | 6.2 |
| g | 9 | 5 | 8 | 14.48 | 5.05 | 3.5 | 1.0 |



was deformed under tension. The asymmetric triangle thus was not suitable for printing unit cells or complex structure, where stacking toolpath would be more challenging. In comparison, a gentle curve at the vertex using the symmetric design toolpath would facilitate 3D printing of unit cell lattice structures. Thus, a symmetric design toolpath with a length of 7 mm for both base dimensions *a* and *b* was further used in the fabrication of multi-cell lattice structures as discussed in more detail below.

3.2 Fabrication of 3D pyramid lattice structure

As shown in Fig. 4a, the bottom path of a triangle lattice truss core was printed along the X direction on the substrate. To print the top path, the print table was first rotated by 90 °. The second triangle lattice truss core was then printed along the X direction as the top path shown in Fig. 4b, where the top and bottom paths were perpendicular to each other and formed a 3D pyramid lattice structure. The vertices of two triangle paths overlapped with each other to form a vertex with the toolpath to print a unit cell sample demonstrated in Fig. 4c. A 3D printed unit cell pyramid lattice structure and 3×3 lattice structure are shown in Fig. 4d and e, respectively.

To validate the degree of curing for the 3D printed composite lattice structures, the DSC analysis was performed. One new contribution of this study was to direct fabricate of 3D lattice structure without post-processing as enabled by the implementation of a high UV laser intensity. With the selected laser spot size, a laser intensity of 33.8 W/cm² was achieved in this study, which was much higher than those reported in previous studies [35, 42] and thus enabled the rapid curing and fabrication of the 3D lattice structures as shown in Fig. 4. It is also important to validate if the high laser intensity was

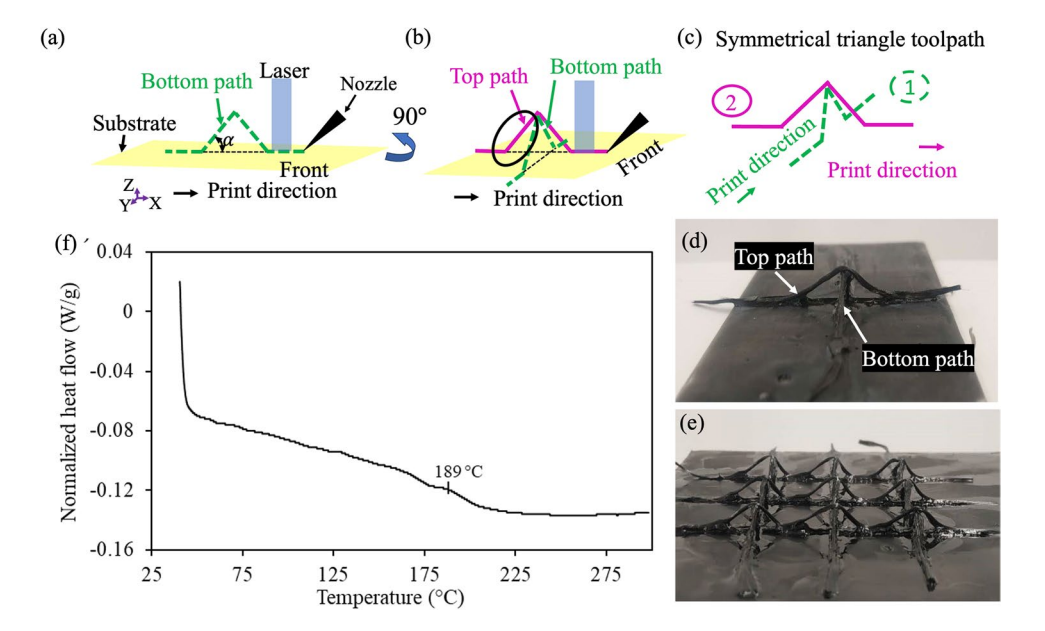
capable of completely curing the thermoset resin, which would result in the improved performance for the composite lattice structure. As shown in Fig. 4(f), no obvious exothermic reaction was observed for the 3D printed thermoset composite samples. This indicated that the laser 3D printing process is capable of completely curing the photopolymer resin within the thermoset composite lattice structure.

3.3 Comparison of compressive mechanical testing and numerical simulations

To measure the mechanical properties of the composite lattice structure, the 2×2 pyramid lattice structure was printed using the toolpath designed in Fig. 5a and was shown in Fig. 5b. The compression test setup is shown in Fig. 5c. The compressive strength values obtained from experimental measurements and numerical simulations are summarized in Fig. 5d with respect to varying fiber volume fractions. A maximum compressive strength of 2.28 MPa and a maximum compressive modulus of 4.48 MPa were observed from the experimental tests at the fiber volume fraction of 31 vol.%. For each fiber volume fraction tested, a good agreement was also found between the experimental results and predicted compressive strength values with a maximum deviation of max 9.2%.

The corresponding stress-strain curves and deformation histories from compression experiments and simulations are illustrated in Fig. 5f-g for the fiber volume fractions of 19 vol.%, 26 vol.%, and 31 vol.%, respectively. The deformed shapes of the lattice unit cells were inset into the stress-strain plots with the predicted von-Mises stress distributions of a typical lattice unit cell under compression highlighted in Fig. 5e with a fiber volume fraction of 31 vol.%.

Fig. 4 3D printing of pyramid lattice structures. a bottom path, (b) top path, (c) schematic diagram of complete symmetric triangle toolpath in preparation of the unit cell lattice structure in (d). (e) 3 × 3 lattice structure. (f) DSC results for the 3D printed thermoset composite samples





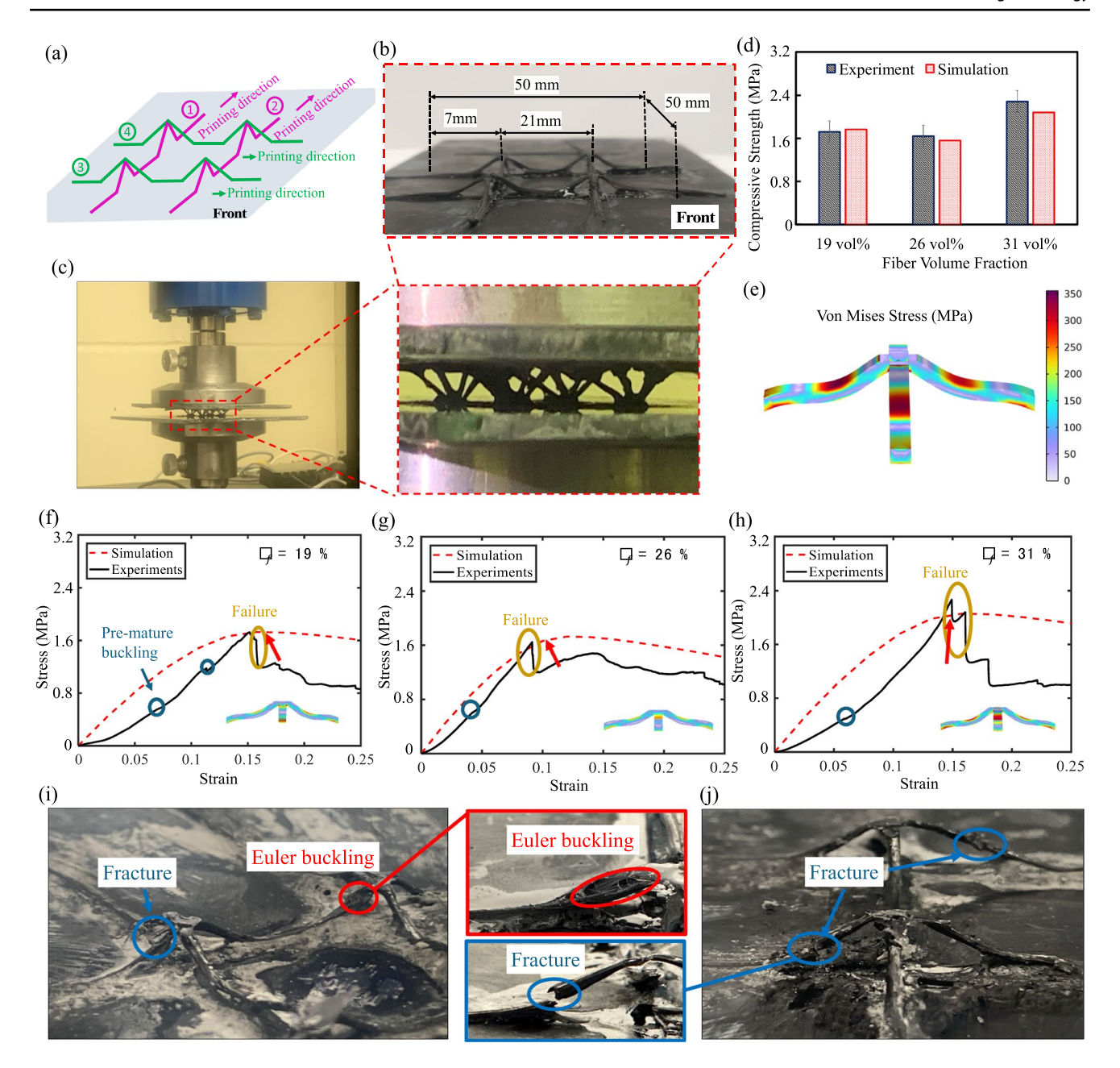


Fig. 5 Mechanical testing and numerical simulations of a 3D printed 2×2 pyramid lattice structure under compression. **a** shows the designed 3D print toolpath. **b** shows a typical 3D printed 2×2 lattice structure. **c** shows the compressive testing process. **d** summarizes compressive strength obtained from experimental measurements and numerical simulations. **e** shows the von Mises stress distribution of a typical lattice unit cell under compression with a fiber volume frac-

tion of 31 vol.%. (f)-(g) show the stress–strain curves obtained from the experiments and the simulations at the fiber volume fractions of 19 vol.%, 26 vol.%, and 31 vol.%, respectively. The corresponding deformed shape of the lattice structures are also included as inset images. (i) and (j) show the typical failures observed within the composite lattice structure samples at the end of the compression tests, including Euler buckling and fracture

The maximum Von-Mises stress location appeared in the middle of the beam in all three cases, which was in accordance with the experimental observed material failure locations. Two typical failure modes were observed as shown in Fig. 5i and j, including fracture and Euler buckling. Fracture mainly occurred in inclined members cured during the upward and downward stages, where the fractured composite

materials exposed CF. Buckling was observed in some of the inclined lattice members. This could be attributed to the uneven distribution of the matrix material or deviation of the 3D printed lattice geometry from the designed symmetric print toolpath, which resulted in nonuniform deformation of the trusses under compression. No obvious damage on the vertex of the samples was observed.



Compared with the simulation results, the stress drop was observed in the experimentally measured stress—strain curves in Fig. 5f-g. This drop represented the failure of the lattice structure, such as Euler buckling and fracture of the composite materials. Since the fracture was not explicitly modeled in the simulations, the stress drop was not observed from the predicted stress—strain curves. Additionally, the drop location was close to the location of buckling in the simulation, which suggested that the fracture was induced by the buckling deformation of the structure. Due to the geometry deviation during 3D printing of the pyramid lattice structure, the experimental results showed different random locations of pre-mature buckling, which was not observed in the simulations with the ideal lattice structures modeled and could be accounted for in the future studies.

4 Conclusions

In this study, a new 3D print method was proposed to direct fabricate lattice structures. By investigating the print toolpath during the 3D printing processes, the geometry of the 3D printed composite pyramid lattice structure was relatively accurately controlled. Through implementations of a high laser intensity of 33.8 W/cm², the 3D composite lattice structures were fully cured and directly prepared with no need of auxiliary tooling or post-processing steps. The 3D printed composite materials were further characterized under compression tests. A maximum compressive strength and compressive modulus of 2.28 MPa and 4.48 MPa were obtained from the experimental measurements. A good agreement was also found between the experimental results and predicted compressive strength values with a maximum deviation of max 9.2%. A comparison between the experiments and simulations suggested that the composite failures were dominated by buckling near the middle sections of the truss structures, which may further lead to the fracture observed from the composite samples after compression tests. The deviation between the experimental measurements and prediction results could be attributed to the non-uniform deposition of the thermoset resin or deviation of the 3D printed lattice structures from the designed toolpath geometries. The findings provided insights in future design and fabrication of high-performance and more complex 3D lattice structures with continuous carbon fiber reinforced thermoset composite materials.

Acknowledgements This material is based upon work supported by the Office of the Under Secretary of Defense for Research and Engineering under award number FA9550-21-1-0226. The authors Y.C. and X.D. acknowledge the partial support from the U.S. Department of Energy Advanced Research Projects Agency–Energy (ARPA-E) under the OPEN 2021 with program award number DE-AR0001576.

Declarations

Competing interests The authors declare that they have no known competing financial interests or personal relationships that could have appeared to influence the work reported in this paper.

References

- Tian X, Todoroki A, Liu T, Wu L, Hou Z, Ueda M, Lu B (2022) 3D printing of continuous fiber reinforced polymer composites: development, application, and prospective. Chin J Mech Eng. 1:100016
- Kopar M, Yildiz A (2023) Experimental investigation of mechanical properties of PLA, ABS, and PETG 3-d printing materials using fused deposition modeling technique. Mater Test 65:1795–1804
- Ning F, Cong W, Hu Y, Wang H (2017) Additive manufacturing of carbon fiber-reinforced plastic composites using fused deposition modeling: Effects of process parameters on tensile properties. J Compos Mater 51:451–462
- Tao W, Leu MC (2016) Design of lattice structure for additive manufacturing. In 2016 International Symposium on Flexible Automation (ISFA). IEEE 325–332
- Nagesha BK, Dhinakaran V, Shree MV, Kumar KM, Chalawadi D, Sathish TJMTP (2020) Review on characterization and impacts of the lattice structure in additive manufacturing. Mater Today: Proc 21:916–919
- Zok FW, Latture RM, Begley MR (2016) Periodic truss structures. J Mech Phys Solids 96:184–203
- Günaydın AC, Yildiz AR, Kaya N (2022) Multi-objective optimization of build orientation considering support structure volume and build time in laser powder bed fusion. Mater Test 64:323–338
- 8. Pan C, Han Y, Lu J (2020) Design and optimization of lattice structures: A review. Appl Sci 10:6374
- Aslan B, Yildiz AR (2020) Optimum design of automobile components using lattice structures for additive manufacturing. Mater Test 62:633–639
- Magerramova L, Volkov M, Afonin A, Svinareva M, Kalinin D (2018) Application of light lattice structures for gas turbine engine fan blades. In Proceedings of the 31st Congress of the International Council of the Aeronautical Sciences. ICAS
- Moon SK, Tan YE, Hwang J, Yoon YJ (2014) Application of 3D printing technology for designing light-weight unmanned aerial vehicle wing structures. Int J Precis Eng Manuf - Green Technol 1:223–228
- Hunt CJ, Morabito F, Grace C, Zhao Y, Woods BK (2022) A review of composite lattice structures. Compos Struct 284:115120
- Yin S, Wu L, Ma L, Nutt S (2012) Hybrid truss concepts for carbon fiber composite pyramidal lattice structures. Compos B Eng 43:1749–1755
- Che L, Xu GD, Zeng T, Cheng S, Zhou XW, Yang SC (2014) Compressive and shear characteristics of an octahedral stitched sandwich composite. Compos Struct 112:179–187
- Li X, Wu L, Ma L, Yan X (2016) Fabrication and mechanical properties of composite pyramidal truss core sandwich panels with novel reinforced frames. J Reinf Plast Compos 35:1260–1274
- Li X, Xiong J, Ma L, Wu L, Yan X (2018) Effect of vacuum thermal cycling on the compression and shear performance of composite sandwich structures containing pyramidal truss cores. Compos Sci Technol 158:67–78



- Yang N, Sun F, Zhu P, Wang J (2024) Mechanical properties of pyramidal lattice sandwich CFRP composites to flat and bending loads. J Reinf Plast Compos 43(3–4):220–232. https://doi.org/10. 1177/07316844231160298
- Fan HL, Meng FH, Yang W (2006) Mechanical behaviors and bending effects of carbon fiber reinforced lattice materials. Arch Appl Mech 75:635–647
- McClintock H, Xiong Z, Rergis B, Lipson H (2023) Design and fabrication of carbon fiber lattices using 3D weaving. Sci Rep 13:14919
- Lee BC, Lee KW, Byun JH, Kang KJ (2012) The compressive response of new composite truss cores. Compos B Eng 43:317–324
- Guan C, Li H, Yang Z, Zhang Y, Fang D (2023) Vibration and damping of carbon fiber reinforced polymer orthogonal lattice truss sandwich panels manufactured by a new manufacturing process. Compos Struct 323:117463
- Ngo TD, Kashani A, Imbalzano G, Nguyen KT, Hui D (2018)
 Additive manufacturing (3D printing): A review of materials, methods, applications and challenges. Compos B Eng 143:172–196
- Maconachie T, Leary M, Lozanovski B, Zhang X, Qian M, Faruque O, Brandt M (2019) SLM lattice structures: Properties, performance, applications and challenges. Mater Des 183:108137
- Zadpoor AA (2019) Mechanical performance of additively manufactured meta-biomaterials. Acta Biomater 85:41–59
- Yan C, Hao L, Hussein A, Young P, Huang J, Zhu W (2015) Microstructure and mechanical properties of aluminium alloy cellular lattice structures manufactured by direct metal laser sintering. Mater Sci Eng, A 628:238–246
- Wang Z, Luan C, Liao G, Yao X, Fu J (2019) Mechanical and self-monitoring behaviors of 3D printing smart continuous carbon fiber-thermoplastic lattice truss sandwich structure. Compos B Eng 176:107215
- Liu S, Li Y, Li N (2018) A novel free-hanging 3D printing method for continuous carbon fiber reinforced thermoplastic lattice truss core structures. Mater Des 137:235–244
- Zhang D, Tian X, Zhou Y, Wang Q, Yan W, Akmal Zia A, ... Li D (2023) Spatial 3D Printing of Continuous Fiber-Reinforced Composite Multilayer Truss Structures with Controllable Structural Performance. Polymers 15: 4333
- Li N, Link G, Jelonnek J (2020) Rapid 3D microwave printing of continuous carbon fiber reinforced plastics. CIRP Ann 69:221–224
- Li N, Link G, Ma J, Jelonnek J (2021) LiDAR based multi-robot cooperation for the 3D printing of continuous carbon fiber reinforced composite structures. In Advances in Manufacturing Technology XXXIV (pp. 125–132). IOS Press
- 31. Zhang P, Han Z, Ran X, Sun S, Fu H (2022) Path design and compression behavior of 3D printed continuous carbon fiber

- reinforced composite lattice sandwich structures. Compos Struct 296:115893
- 32. He X, Ding Y, Lei Z, Welch S, Zhang W, Dunn M, Yu K (2021) 3D printing of continuous fiber-reinforced thermoset composites. Addit Manuf 40:101921
- Ming Y, Zhang S, Han W, Wang B, Duan Y, Xiao H (2020) Investigation on process parameters of 3D printed continuous carbon fiber-reinforced thermosetting epoxy composites. Addit Manuf 33:101184
- Rahman MA, Islam MZ, Gibbon L, Ulven CA, La Scala JJ (2021)
 printing of continuous carbon fiber reinforced thermoset composites using UV curable resin. Polym Compos 42:5859–5868
- Abdullah AM, Ding Y, He X, Dunn M, Yu K (2023) Direct-write 3D printing of UV-curable composites with continuous carbon fiber. J Compos Mater 57:851–863
- Jiang H, Abdullah AM, Ding Y, Chung C, Dunn ML, Yu K (2023)
 Printing of continuous fiber composites using two-stage UV curable resin. Mater Horiz 10:5508–5520
- Yourdkhani M, Dojan C, Ziaee M, Radosevich S (2023) Additive manufacturing of carbon fiber-reinforced thermoset composites via in-situ thermal curing, PREPRINT (Version 1). Available at Research Square. https://doi.org/10.21203/rs.3.rs-3397066/v1
- Tian X, Liu T, Yang C, Wang Q, Li D (2016) Interface and performance of 3D printed continuous carbon fiber reinforced PLA composites. Compos A Appl Sci Manuf 88:198–205
- Zhao X, Liu A, Zhou L, Yang Z, Wei S, Zhao Z, ... Ma L (2022)
 3D printing of bioactive macro/microporous continuous carbon fibre reinforced hydroxyapatite composite scaffolds with synchronously enhanced strength and toughness. J Eur Ceram Soc 42: 4396–4409
- Thakur A, Dong X (2020) Additive manufacturing of 3D structural battery composites with coextrusion deposition of continuous carbon fibers. Manuf Lett 26:42–47
- Pappas JM, Thakur AR, Leu MC, Dong X (2021) A parametric study and characterization of additively manufactured continuous carbon fiber reinforced composites for high-speed 3D printing. Int J Adv Manuf Technology 113:2137–2151
- Rau DA, Reynolds JP, Bryant JS, Bortner MJ, Williams CB (2022)
 A rheological approach for measuring cure depth of filled and unfilled photopolymers at additive manufacturing relevant length scales. Addit Manuf 60:103207

Publisher's Note Springer Nature remains neutral with regard to jurisdictional claims in published maps and institutional affiliations.

Springer Nature or its licensor (e.g. a society or other partner) holds exclusive rights to this article under a publishing agreement with the author(s) or other rightsholder(s); author self-archiving of the accepted manuscript version of this article is solely governed by the terms of such publishing agreement and applicable law.

